Canadian Science Publishing | Canadian Journal of Chemistry

Simultaneous reduction of Cr (VI) and degradation of azo dyes by F-Fe-codoped TiO_2/SiO_2 photocatalysts under visible and solar irradiation

Journal:	*Canadian Journal of Chemistry*
Manuscript ID	cjc-2018-0529.R1
Manuscript Type:	Article
Date Submitted by the Author:	28-Mar-2019
Complete List of Authors:	Ghanbari, Sina; Islamic Azad University Science and Research Branch Givianrad, Mohammad Hadi; Islamic Azad University Science and Research Branch Aberoomand Azar, Parviz; Islamic Azad University Science and Research Branch
Is the invited manuscript for consideration in a Special Issue?:	Not applicable (regular submission)
Keyword:	Hexavalent chromium, Dye degradation, Photocatalyst, Photoreactor, Codoped TiO₂

SCHOLARONE™
Manuscripts

Simultaneous reduction of Cr (VI) and degradation of azo dyes by F-Fe-codoped TiO_2/SiO_2 photocatalysts under visible and solar irradiation

Sina Ghanbari, Mohammad Hadi Givianrad*, Parviz Aberoomand Azar

Department of Chemistry, Science and Research Branch, Islamic Azad University, Tehran, Iran

*Corresponding author: Mohammad Hadi Givianrad
Email Address: givianradh@yahoo.com
Telephone Number: +982144868449

Draft

Abstract

A new TiO_2/SiO_2 photocatalyst codoped with fluorine and iron was synthesized using sol-gel process and immobilized onto glass beads using coupling two methods of dip-coating and heat attachment. The prepared samples were characterized by XRD, FT-IR, DRS-UV/Vis, FESEM, EDX, TEM and N_2 Adsorption/Desorption analysis. The effective parameters of pH, flow rate and photoreactor vessels' angle against solar irradiation on degradation performance were optimized. Subsequently, the photocatalytic activity of the prepared nanocomposites was investigated in an innovative fabricated photoreactor using a four-component pollutant mixture of Cr (VI), basic red 29, basic blue 41 and basic yellow 51, under visible and solar irradiation. Furthermore, the effectiveness of photoreactor performance was assessed under various outdoor climate conditions as natural irradiation source. Consequently, UV/Vis spectrophotometry results showed significant efficiency of photocatalytic removal of the pollutants mixture. TOC results of 74.39% and 78.04% for removal of organic content of the sample under visible and solar light, respectively, were also confirmed the great capability of the designed system for the simultaneous removal of some hazardous inorganic and organic contaminants under natural light sources.

Keywords: Hexavalent chromium; Dye degradation; Photocatalyst; Photoreactor; Codoped TiO_2

Draft

1. Introduction

Nowadays, due to industrializing societies, environmental pollutants have become a great concern. Heavy metals like Cr (VI) and dyes, made by industrial processes such as paint making, leather tanning and others, are some of the most widespread pollutants in wastewaters [1,2]. Between the two common oxidation states of chromium, Cr (VI) is highly toxic and carcinogenic agent, while Cr (III) is readily adsorbed or precipitated at neutral or alkaline pH [3–5]. Therefore, reduction of Cr (VI) to its less toxic and less mobile state, Cr (III), has attracted much attention [6,7]. Since azo dyes are extensively used in dyeing industries, great emphasis has been given on their removal [7]. These dye molecules are hardly biodegradable and chemically stable, although they have potential to anaerobically transform to hazardous aromatic amines [7,8]. Simultaneous removal of these inevitably coexisting pollutants in industrial wastewaters has been investigated in recent decades [9,10].

Removal of these pollutants has been studied by two major approaches including adsorption and photocatalysis. Using mesoporous aluminum magnesium oxide composites for arsenic remediation [11], flowerlike WSe_2 and WS_2 microspheres for Pb^{2+} and Hg^{2+} removal [12] and coral reef-like carbon nitrides for heavy metal ion adsorption [13] are some of the advantages of using adsorbents in wastewater treatment process. Photocatalytic treatment of industrial wastewaters using MOFs, ZnO and TiO_2 is one of the other interesting approaches in the last decade [14–16]. Using perovskite photocatalysts with some novel modifications has also attracted much attention for hydrogen evolution in aqueous solutions [17,18].

TiO_2, as an advantageous photocatalyst can be applied in various photoremoval systems with high efficiency. This substrate is widely used to eliminate the aqueous and also gaseous pollutions [19]. Titania, owing to the wide band gap of its the most activated polymorph, anatase, needs some modifications to be able to perform photocatalytic process under visible and solar lights [10,20,21]. Doping metals and non-metals have been pursued to sensitize titania toward visible and solar irradiation [22,23].

Recently, anion-doped TiO_2 such as N, S, B, F with relatively high photocatalytic activity under visible light irradiation have been investigated [24–28]. Doping with non-metals has been considered a great approach as a consequence of the effectiveness and simplicity of the process in addition to abundance of dopants [29]. Among these anion-dopants, some studies reported the great effect of fluorine on increasing of surface acidity and enhancing the adsorption of agents [30,31]. The crystallinity of anatase was also improved with fluorine due to suppressing the formation of brookite phase as well as preventing any phase transitions to rutile [32]. Presence of some metals also has been studied and has significantly influenced titania's property [33–35]. Incorporation of transition metals such as Fe, Co, Ni, Pt in TiO_2 lattice can result in new energy levels' formation [36]. Iron is one of the most promising metal-dopant due to formation of new energy levels and trapping the photogenerated electrons and also inhibiting the electron-hole recombination [37]. Moreover, to further improvements of photocatalytic activity, codoping of metals, non-metals or a mixed of both have attracted more attention [38–40]. One of the other effectual activities to increase the photocatalytic efficiency is increasing the surface active sites of TiO_2 by combining it with

other semiconductors [41]. Silicon dioxide is one of the most effective agents in combination with titanium dioxide due to increasing the specific surface area, decreasing the band gap and suppressing anatase phase transformation to rutile in the prepared photocatalyst [42].

One of the major problems which the studies in this field are face is scaling up the process and examining the capability of the proposed treatment system in the real world natural conditions. Some attempts have been accomplished to fulfill the lack of such studies out of the controlled environment of laboratories and have been virtualize the treatment process [43].

The aim of this study is evaluating photocatalytic activity of synthesized F-Fe-codoped TiO_2/SiO_2 (FFeTS) immobilized on glass beads by a fabricated fixed bed photoreactor under visible and solar irradiation. The experiments performed on an aqueous solution of hexavalent chromium and three azo dyes including basic red 29, basic blue 41 and basic yellow 51 as a model.

2. Experimental

2.1. Synthesis and immobilization

All the chemicals were purchased from Merck and used without any further purification. Tetrabutyl orthotitanate (TBOT), ammonium fluoride and Iron (III) nitrate were used as Titania, fluorine and iron precursors, respectively. To prepare the sol, 5 mL TBOT, 20 mL absolute ethanol and 5 mL acetylacetone were mixed. After 30 min of vigorous stirring, 4 mL deionized water was added and the stirring continued for another 10 min. Then, the pH was adjusted at about 1.8 with concentrated HCl. Ammonium fluoride and iron (III) nitrate nonahydrate in the appropriate molar ratios (F/Ti = 0.2, Fe/Ti = 0.02) were added while stirring [44–46]. Followed by 2 h of stirring, 5 g silica gel as a silicon source was added to the mixture and stirring continued for another 2 h and the sol got ready for the coating process.

Coating the glass beads (1 mm in diameter) was performed by coupling dip coating and heat attachment methods. Prior to the process, the glass beads were etched in diluted HF for 24 h. Then, the beads were washed with deionized water and dried at 100 ˚C for 4 h. The beads were prepared as it described and became ready for coating process. To do so, the beads were immersed in the sols for 30 min. After getting out of the sol, dried with hair dryer and immersed again for another 30 min. The beads were dried in oven for 4 h at 80 ˚C. Finally, the calcination was performed at 500 ˚C for 1 h to yield FFeTS photocatalysts. To gain the more stability of the nanoparticles onto the beads, heat attachment process was performed followed by heating at 150 ˚C for 2 h. Pristine TiO_2/SiO_2, coated on glass beads, was prepared as above mentioned method.

2.2. Evaluation of photocatalytic activity

Photocatalytic activities were evaluated on an aqueous mixture containing 30 mg L^{-1} of each three azo dyes (basic red 29, basic blue 41 and basic yellow 51) and 5 mg L^{-1} Cr (VI) ($K_2Cr_2O_7$ solution). The fabricated photoreactor consisted of 7 glass tubes (ID = 10 mm, L = 200 mm) filled with photocatalyst coated glass beads for laboratory scale experiments. The tubes were placed against a mirror to supply the light for the photocatalysts behind the light source. All the set-ups were positioned over an adjustable surface to adjust the angle of vessels in front of the sunlight,

vertically. The visible power source of the photoreactor was an OsramPowerstar® HQI®-BT 400 W/D Pro lamp equipped with a UV filter and also a ballast device to ensure gaining a constant current in the used light source. The distance between the visible source and the vessels was fixed as 10 cm in all experiments. The photocatalytic experiments under solar irradiation were performed in clear sky during July to September at the Science and Research Branch, Islamic Azad University in Tehran (latitude and longitude: 35.79084, 51.31581). The degradation efficiencies of model azo dyes including basic red 29, basic blue 41 and basic yellow 51 were identified by spectrophotometric method in 506, 607 and 411 nm wavelength of maximum absorbance, respectively. The reduction of Cr (VI) was accomplished through 1,5–diphenylcarbazide colorimetric method by forming purple complex at 544 nm followed by subtracting technique to eliminate the interference of dyes [10]. Due to the avoidance of presence of HCl in Cr (VI) detection method, the pH of the solutions was adjusted with 1 M H_2SO_4 and 1 M NaOH [47]. The removal amounts of the pollutants were measured by Varian Cary300 UV/Vis spectrophotometer. Subsequently, total organic carbon of the samples, before and after the degradation process was determined by Hach DR5000 spectrophotometer. Finally, total chromium of the treated wastewater was measured by Varian SpectraAA200 flame atomic absorption spectrometer (FAAS).

2.3. Characterization

The X-ray diffraction (XRD) pattern of the samples were obtained by a Seifert 3003 PTS X-ray diffractometer using Cu Kα radiation as the X-ray source in 2θ range of 15-90˚. The FT-IR spectra of the samples were determined by Thermo Nicolet Nexus 870 spectrometer. The diffuse reflectance UV/Vis (DRS-UV/Vis) spectra of the prepared photocatalysts were prepared by Avantes Avaspec-2048-TEC spectrophotometer. The morphology of the photocatalysts were observed by MIRA3 TESCAN-XMU field emission scanning electron microscope (FESEM) equipped with an energy dispersive X-ray (EDX). The Transmission electron microscopy (TEM) images were obtained by a Philips CM30 at 150KV. The N_2 adsorption and desorption isotherms were measured using Belsorp mini II. The specific surface area and pore size distribution were measured from the adsorption isotherms using Brunauer-Emmett-Teller (BET) and Barret-Joyner-Halender (BJH) methods, respectively.

3. Results and discussion

3.1. X-ray diffraction (XRD) analysis

XRD pattern of the prepared samples was obtained to investigate the phase structure of the nanoparticles. Between the three polymorphs of TiO_2, anatase is the most activated one in photocatalytic activity that was confirmed by (1 0 1), (0 0 4), (2 0 0), (1 0 5) and (2 1 1) diffraction peaks (JCPDS 21-1272) [44,48]. As shown in Fig. 1, all the samples were synthesized in anatase phase, without the other two phases of TiO_2, brookite and rutile. As it was expected, the crystallinity of anatase was improved with fluorine and silicon dioxide due to suppressing the

brookite and rutile phase formation [32]. The crystalline sizes of the prepared photocatalysts were calculated using Debye-Scherrer equation at the main peak of anatase TiO_2 (2θ =25.2˚) (Eq. (1)).

$$D = \frac{0.89\,\lambda\,180}{\pi\,\beta\,\mathrm{Cos}\theta} \quad (1)$$

Where D is the crystal size of the synthesized photocatalysts, λ is the X-ray wavelength (0.154 nm), β is the full width at half maximum (FWHM) of the diffraction peak in radian. Average crystal sizes of FFeTS and pure TiO_2 were calculated to be 12 nm and 11 nm, respectively.

Fig. 1

3.2. FT-IR spectroscopy analysis

Fig. 2 shows the FT-IR spectra of the prepared samples. The presence of hydroxyl ion bending vibrations and adsorbed water were confirmed by the peaks at 3408.21 cm^{-1} and 1634.55 cm^{-1}, respectively. The strong peak at 1098.16 cm^{-1} shows the stretching vibrations of Si-O-Si and the peak at 930 cm^{-1} is related to the Si-O-Ti bonds in the TiO_2 lattice [49]. As it was observed, the peaks below 900 cm^{-1} are corresponds to the Ti-O flexion vibrations [44].

Draft

Fig. 2

3.3. UV/Vis diffuse reflectance spectra (DRS)

As it is clearly observed in the UV/Vis DRS spectra of the synthesized catalysts (Fig. 3), doping fluorine and iron in the TiO_2 lattice, was yielded to a red shift in the absorption edge of the undoped TiO_2. The success of such a doping can improve the activity of prepared photocatalysts in contrast with pure TiO_2, in the visible region. The band gap also calculated by the following equation (Eq. (2)) [50]:

$$E_g = \frac{h\,C}{\lambda} \quad (2)$$

where E_g is the band gap energy of catalysts, h is Planck's constant, C is the speed of light in vacuum and λ is the wavelength of related absorption edge. As it was described, the band gap energy of the FFeTS and undoped TiO_2 was 2.87 eV and 3.18 eV, respectively.

Fig. 3

3.4. FESEM and EDX analysis

The surface morphology of the prepared photocatalysts was investigated by FESEM images. As shown in the Fig. 4b, the prepared FFeTS catalysts are globular and uniform without any agglomerations as a comparison with undoped TiO_2, which the severe agglomeration is clearly observed (Fig. 4a). The morphology of the surface appears to be rough that it is a benefit during photocatalytic activity owing to the increase of the active sites facing the pollutants.

The composition of the synthesized photocatalyst was determined by EDX analysis (Fig. 5). It was observed that doping fluorine and iron were successfully performed into TiO_2 lattice.

Fig. 4
Fig. 5

3.5. TEM analysis

The TEM images of FFeTS were presented in Fig. 6. The results are in good agreement with FESEM results and showed high globularity and the absence of any agglomeration of the prepared nanoparticles.

Draft

Fig. 6

3.6. N_2 Adsorption/desorption analysis

Nitrogen physical adsorption method was used to investigate the surface area and porosity distribution of as-prepared nanocomposites. According to IUPAC classification, the isotherm of FFeTS nanocomposites showed a typical IV-like with an H2 hysteresis indicating the presence of mesoporous structure (Fig. 7) [51]. BJH pore size distribution curve of FFeTS from the adsorption branch was shown at the inset of Fig. 7 and clearly indicates the mesoporous structure. Table 1 tabulated the average pore size and BET results of prepared nanocomposites with and without presence of SiO_2. The results were showed that doping F, Fe and Si have not changed the content of average pore diameter while significantly increased the surface area of FFeTS nanocomposites.

Fig. 7
Table 1

3.7. Photocatalytic activities

General descriptions about the basis and mechanism of heterogeneous photocatalysis under various light sources have been discussed previously [7,52,53]. However, as a brief summary, irradiation of TiO_2 in an aqueous matrix with light energy greater than its band gap ($h\upsilon > E_g = 3.2$ eV) results electrons at conduction band and holes at valance band (Eq. (3)):

$$TiO_2 + h\nu \xrightarrow{\lambda < 400\ nm} e_{cb}^- + h_{vb}^+ \quad (3)$$

The photogenerated valance band holes can react with the adsorbed water to produce hydroxyl radicals (Eq. (4)). The produced hydroxyl radicals as well as valance band holes can undergo photocatalytic reaction with the target pollutants (Eqs. (5) and (6)). On the other hand, the photogenerated conduction band electrons can react with adsorbed molecular oxygen on TiO_2 to form superoxide radical anions (Eq. (7)). The formed superoxide radical anions parallel to conduction band electrons can also react with the target pollutants to produce degradation and reduction products (Eqs. (8) and (9)) [54–56].

$$h_{vb}^+ + H_2O_{(ads)} \rightarrow HO^\bullet + H^+ \quad (4)$$

$$HO^\bullet + \text{target pollutant} \rightarrow \text{degradation product} \quad (5)$$

$$h_{vb}^+ + \text{target pollutant} \rightarrow \text{oxidation product} \quad (6)$$

$$e_{cb}^- + O_2 \rightarrow O_2^{\bullet -} \quad (7)$$

$$O_2^{\bullet -} + \text{target pollutant} \rightarrow \text{degradation product} \quad (8)$$

$$e_{cb}^- + \text{target pollutant} \rightarrow \text{reduction product} \quad (9)$$

The mechanism of simultaneous removal of Cr (VI) and azo dyes was illustrated schematically in Fig. 8. To accomplish the removal process of the pollutants, two pathways of oxidation for the organic pollutants and the reduction for Cr (VI) will be noted. The process of Cr (VI) reduction owing to its dependence to pH will be described under pH optimization section. To the best of our knowledge, the degradation pathway of azo dyes is corresponded to the produced free radicals of Reactive Oxygen Species (ROSs) owing to their attack to the N=N bond of azo dyes. So, the broken molecules have less π-π bonds' conjugated degree rather than the main dye molecules. Consequently, these molecules will be oxidized to the nontoxic H_2O and CO_2 with the reaction progress. Some previous literatures were also proposed this pathway of dyes degradation [57,58]. The decrease in the organic content of the treated wastewater evaluated by TOC analysis, was also in good agreement with the suggested mechanism.

Fig. 8

The photocatalytic activity investigations were performed on a mixture of 30 mg L^{-1} of each three azo dyes and 5 mg L^{-1} Cr (VI) under visible light and solar irradiation. Owing to the adjustability feature of the fabricated photoreactor in outdoor conditions, the outdoor experiments, under solar irradiation, were performed in three different angles in front of the sun irradiation (30˚, 45˚ and 60˚ vertically). Comparative experiments in both conditions were performed to investigate

the removal efficiencies of pristine TiO_2/SiO_2, single and codoped TiO_2/SiO_2 in the presence and absence of light source. To evaluate the best condition for removal efficiencies, three factors of pH, flow rate and photoreactor vessels' angle against sunlight were investigated. In order to verify the repeatability of photocatalytic degradations, all of the experiments were performed three times and the results were reported with error bars in the figures.

The optimization of each parameter was performed due to the natural experimental conditions. pH values were selected somehow to cover all ranges of pH values as well as basic, neutral and acidic. As it was understood by Cr (VI) transformation mechanism and its dependence to pH, described in the following section, the working pH values at basic conditions were not chosen more than 9. On the other hand, owing to the measurements on the pH of real wastewaters at about 3, and with respect to performing the experiments in the conditions close to reality, the low range of pH was selected as 3. Flow rate was also selected as the controllable conditions. Owing to the adjustable power of peristaltic pump and the novel design of the photoreactor to work in natural conditions, higher flow rates were achieved than former studies. But at the flow rates of 420 and 560 mL min^{-1}, there was a really hard inner pressure that might face the reactor to some damages. Subsequently, the ranges of working flow rate were selected at the highest possible values. The angle of the photoreactor against solar irradiation was also selected the way that three different positions could be examined. At the higher degrees than 60°, the vessels would not completely fill with the sample due to the flattening the photoreactor's vessels. Thus, there was always some extent of nanocomposites that were not in contact with the samples. Consequently, the selected ranges were chosen to accomplish the experiments.

3.7.1. Effect of pH

The experiments were performed at the pH of 3, 5, 7 and 9. As shown in Fig. 9, it was found that the degradation of dyes and reduction of Cr (VI) efficiencies strongly depends on pH of the solution. The results showed the decrease in the removal efficiencies of both dyes and Cr (VI) in neutral and alkaline pH. The mechanism occurred during the photocatalytic process could be understood by combination of two parameters including the photocatalyst surface and the target molecules. As it was previously mentioned, solution's pH plays an important role in the mechanisms pathway. Due to the point of zero charge for TiO_2 at the pH about 5.9, the surface can act an amphoteric behavior at different pH conditions. According to the Eqs. (10) and (11), Ti—OH, representing primary hydrated substrate, become negatively charged at above the pH of TiO_2 point of zero charge [59,60].

$$Ti—OH + H^+ \rightleftharpoons Ti—OH_2^+ \quad (10)$$

$$Ti—OH + HO^- \rightleftharpoons Ti—O^- + H_2O \quad (11)$$

It means that at greater pH values than 5.9, the anionic surface of the catalyst would prevent the anionic dyes to adsorb on the surface to cooperate the degradation process. This fact would imply the decrease in the degradation efficiencies of the stated basic dyes at alkaline pH. On the contrary, at acidic pH values, the positively charged surface would electrostatically attract the target anions to participate the degradation process that would result the increase of removal efficiencies.

https://mc06.manuscriptcentral.com/cjc-pubs

On the other hand, based on the Eq. (12) in aqueous solutions, $Cr_2O_7^{2-}$ anions collaborate the following equilibrium [61]:

$$Cr_2O_7^{2-} + H_2O \rightleftharpoons 2HCrO_4^- \rightleftharpoons 2CrO_4^{2-} + 2H^+ \quad (12)$$

The concentration of the mentioned various anions highly depends on the pH. Particularly, at pH around 2.5, the most dominant anions are $Cr_2O_7^{2-}$ and $HCrO_4^-$. However, at pH about 6.5, the most dominant species are $HCrO_4^-$ and CrO_4^{2-} anions whereas there is almost no electrostatic attraction among them due to the point of zero charge of the surface [61,62]. At acidic conditions, the electrostatic attraction between the positively charged surface and Cr (VI) anions on one hand and capturing the photogenerated conduction band electrons by them on the other hand results to their reduction as follows (Eqs. (13) and (14)) [7,9]:

$$HCrO_4^- + 7H^+ + 3e_{cb}^- \rightarrow Cr^{3+} + 4H_2O \quad (13)$$
$$Cr_2O_7^{2-} + 14H^+ + 6e_{cb}^- \rightarrow 2Cr^{3+} + 7H_2O \quad (14)$$

While according to following reaction, Cr (III) tends to form a stable precipitate at the pH values above 4-5 (Eq. (15)):

$$CrO_4^{2-} + 4H_2O + 3e_{cb}^- \rightarrow Cr(OH)_3 + 5HO^- \quad (15)$$

Precipitating of Cr $(OH)_3$ on the catalysts surface will occupy the surface active sites and results to the decrease in removal efficiencies.

The results also showed that the degradation efficiencies of the dyes due to their anionic structure, were increased with the decrease of pH. As it was reported elsewhere, degradation of azo dyes is higher in low pH [63,64]. Due to achieve the highest removal efficiencies, for the model pollutants mixture, the working pH selected at 3 for the rest of experiments.

Fig. 9

3.7.2. Effect of flow rate

Effect of the solution's flow rate, a common factor reported in continuous-flow photoreactors, was investigated. Fig. 10 shows the removal efficiencies at the flow rates of 140, 280, 420 and 560 mL min^{-1}. The results demonstrate that there is not any considerable difference between the degradation efficiencies in the chosen flow rates. At lower flow rates, the interaction time of the pollutant molecules and the TiO_2 surface will increase and that would be a beneficial point. But, with respect to the presence of Cr (VI) in the pollutant mixture, the possibility of its trapping into the pores of photocatalytic substrate is unavoidable. Thus, at the flow rate of 140 mL

min^{-1}, 99.02% of Cr (VI) was seemed to be completely transformed to Cr (III). But the experiments on measurement of total chromium by FAAS proved the adsorption occurred on the surface of the photocatalyst. Active site occupation performed by chromium was also resulted to decrease in the photodegradation percentage of the azo dyes. On the other hand, at higher flow rates it was suggested that the circulation of the solution will force the pollutants to move toward the new active sites more and more, but the interaction time between the pollutant and photocatalysts surface would be decreased. Therefore, with the increase of flow rate the transformation of Cr (VI) to Cr (III) and photodegradation of azo dyes were decreased. Subsequently, the optimum flow rate was selected due to achieve a mutual agreement between the two parameters of active sites occupation and interaction time. It is a significant point especially, while working on a combination of pollutants with the risk of adsorption and occupation of the photocatalysts surface active sites. Consequently, the flow rate of 280 mL min^{-1} with the highest efficiency was selected.

Fig. 10

3.7.3. Effect of photoreactor vessels' angle against sunlight

One of the most important factors for evaluating the outdoor performance of the fabricated photoreactor is to optimize the vessel's angle against the sun irradiation. Hereto, the vessels' angle was adjusted to 30˚, 45˚ and 60˚ vertically and the photocatalytic removals were investigated. As shown in Fig. 11, owing to less incoming irradiation at 30˚, the removal efficiencies are lower than the other two conditions. At 60˚, the removal of Cr (VI) was not so fast but the decrease in the amount of chromium was observed. Alternatively, the photodegradation of azo dyes were obviously decreased. It can conclude that flattening the slope of the photoreactor vessels at 60˚ against vertical line can cause surface active sites' occupation owing to the trapping of Cr (VI) on the substrate. So the decrease in the degradation of dyes was occurred. Hence, the degree of 45˚ was chosen for the further experiments under solar irradiation.

Fig. 11

The removal efficiencies of dyes degradation and Cr (VI) reduction were calculated by the following reaction (Eq. (16)):

$$\% \text{ Removal} = \frac{C_0 - C_t}{C_0} \times 100 \quad (16)$$

Where C_t is the concentration of pollutant at the corresponding time and C_0 is the initial concentration of the pollutant.

Fig. 12, demonstrates the removal efficiencies of the pollutants in different conditions of visible irradiation. As it is clear, the degradation and reduction efficiencies were negligible in dark condition. This will imply that no adsorption was occurred on the catalyst surface and entire the removal process was in consequence of photocatalysis. The low amount of adsorption is suggested to be the result of glass beads surface porosity. The investigations on removal efficiencies in the absence of photocatalyst also showed that all of the pollutants were completely stable in the environment and there were no spontaneous degradations or transformations in the absence of catalyst. Comparative studies were also performed on pristine TiO_2/SiO_2 to confirm the enhancing effect of doping F and Fe on photocatalytic activity of the prepared substrate. As it is obvious, the results indicate doping fluorine and iron have significantly increased the activity of the prepared catalyst in visible region.

Fig. 12

The degradation of azo dyes and reduction of Cr (VI) efficiencies in different conditions of solar irradiation have demonstrated in Fig. 13. The photocatalytic experiments were performed at the optimized angle and the higher removal of the pollutants was observed. At the same conditions, removal efficiencies were also investigated upon pristine TiO_2/SiO_2.

Fig. 13

For the purpose of understanding the synergistic effect of doping F and Fe on photoremoval of the pollutants, comparative studied were performed on F-TiO_2/SiO_2 and Fe-TiO_2/SiO_2 under visible and solar irradiations (Figs. 14 and 15). It was concluded based on the results that codoping the elements will increase the photocatalytic activity of the prepared catalyst in order to accomplish photoremoval of the pollutants. This effect may be the result of collaboration of the presence of a metal and non-metal on lowering the band gap of pure titania.

Fig. 14
Fig. 15

https://mc06.manuscriptcentral.com/cjc-pubs

In order to find out the efficiency of the fabricated system in different environmental conditions, the photodegradation and photoreduction of the pollutants were also investigated under semi-cloudy sky. The results shown in Fig. 16, confirmed the high performance of such system in wastewater treatment with complex matrices.

Fig. 16

Investigations to understand the repeatability and durability of the prepared substrates were also performed. As shown in Fig. 17, the photodegradation results were decreased to about 90% after fourth 12 h cycle and the removal efficiencies were decreased to 70% after seventh cycle. Accordingly, the results showed the great efficiency of the fabricated system after several working cycles.

Fig. 17

Draft

To make sure the removal of organic pollutants of the wastewater, TOC analysis was performed on the samples, before and after the photocatalytic process. The results showed the percentage removal of organic content of the sample under visible and solar light, at 74.39% and 78.04%, respectively. Investigations on the adsorption of chromium was accomplished by FAAS analysis and showed the 0.971 mg L^{-1} of chromium adsorption owing to the porosity of the glass beads' surface.

4. Conclusion

The simultaneous photodegradation of three azo dyes and photoreduction of Cr (VI) were investigated upon TiO_2/SiO_2 photocatalysts doped with fluorine and iron in a fabricated photoreactor under visible and solar irradiation. The prepared nanoparticles were strongly coated on glass beads' substrate via dip coating and heat attachment methods. The results of the characterization confirmed the fully anatase structure, amplified activity in the visible region, enhanced electron-hole recombination as well as uniform and globular morphology of the synthetized nanocomposites. The effective parameters of pH, flow rate and vessels' angle of the reactor against sunlight were also optimized. Subsequently, the best removal condition of the pollutant mixture was attainable at acidic pH, flowrate of 280 mL min^{-1} and the angle of 45° against solar irradiation. The mechanisms of the photocatalytic reaction owing to the great influence of pH on the removal extents of the pollutants were also discussed. The innovative and novel system showed a significant efficiency in the decontamination of four-component hazardous pollutant mixture of Cr (VI), basic red 29, basic blue 41 and basic yellow 51, in different outdoor climate

conditions, higher flow rates and different angles against sunlight which might be a great promising possibility to photodegradation of more complex pollutants in natural climate conditions under visible and solar irradiation as a green source.

Acknowledgment

The authors gratefully appreciate the hard work of the staff of Razi Laboratory Complex of Islamic Azad University, Science and Research Branch.

References

(1) Fu, F.; Wang, *J. Environ. Manage*. **2011**, *92*, 407. doi: 10.1016/j.jenvman.2010.11.011.
(2) Robinson, T.; McMullan, G.; Marchant, R.; Nigam, P., *Bioresource Technol*. **2001**, *77*, 247. doi: 10.1016/S0960-8524(00)00080-8.
(3) Schrank, S. G.; Jose, H. J.; Moreira, R. F. P. M., *J. Photochem. Photobiol. A Chem.* **2002**, *147*, 71. doi: 10.1016/S1010-6030(01)00626-8.
(4) Barrera-Diaz, C. E.; Lugo-Lugo, V.; Bilyeu, B., *J. Hazard. Mater*. **2012**, *223*, 1. doi: 10.1016/j.jhazmat.2012.04.054.
(5) Yang, J.-K.; Lee, S.-M., *Chemosphere* **2006**, *63*, 1677. doi: 10.1016/j.chemosphere.2005.10.005.
(6) Yang, J. K.; Lee, S. M.; Farrokhi, M.; Giahi, O.; Shirzad Siboni, M., *Desalin. water Treat.* **2012**, *46*, 375. doi: 10.1080/19443994.2012.677564.
(7) Papadam, T.; Xekoukoulotakis, N. P.; Poulios, I.; Mantzavinos, D., *J. Photochem. Photobiol. A Chem.* **2007**, *186*, 308. doi: 10.1016/j.jphotochem.2006.08.023.
(8) Mantzavinos, D.; Psillakis, E., *J. Chem. Technol. Biot*. **2004**, 79, 431. doi: 10.1002/jctb.1020.
(9) Yang, Y.; Wang, G.; Deng, Q.; Ng, D. H. L.; Zhao, H., *ACS Appl. Mater. Interfaces* **2014**, *6*, 3008. doi: 10.1021/am405607h.
(10) Wang, Q.; Chen, X.; Yu, K.; Zhang, Y.; Cong, Y., *J. Hazard. Mater.* **2013**, *246*, 135. doi: 10.1016/j.jhazmat.2012.12.017.
(11) Li, W.; Chen, D.; Xia, F.; Tan, J. Z. Y.; Huang, P.-P.; Song, W.-G.; Nursam, N. M.; Caruso, R. A., *Environ. Sci. Nano* **2016**, *3*, 94. doi: 10.1039/C5EN00171D.
(12) Li, W.; Chen, D.; Xia, F.; Tan, J. Z. Y.; Song, J.; Song, W.-G.; Caruso, R. A., *Chem. Commun.* **2016**, *52*, 4481. doi: 10.1039/C6CC00577B.
(13) Tan, J. Z. Y.; Nursam, N. M.; Xia, F.; Sani, M.-A.; Li, W.; Wang, X.; Caruso, R. A., *ACS Appl. Mater. Interfaces* **2017**, *9*, 4540. doi: 10.1021/acsami.6b11427.
(14) Pandikumar, A.; Ramaraj, R., *J. Hazard. Mater.* **2012**, *203*, 244. doi: 10.1016/j.jhazmat.2011.12.019.
(15) Zhang, Z.; Xu, Y.; Ma, X.; Li, F.; Liu, D.; Chen, Z.; Zhang, F.; Dionysiou, D. D., *J. Hazard. Mater.* **2012**, *209*, 271. doi: 10.1016/j.jhazmat.2012.01.021.
(16) Song, F.; Li, W.; Sun, Y., *Inorganics* **2017**, *5*, 40. doi: 10.3390/inorganics5030040.
(17) Guan, Z.; Wu, Y.; Wang, P.; Zhang, Q.; Wang, Z.; Zheng, Z.; Liu, Y.; Dai, Y.; Whangbo, M. H.; Huang, B., *Appl. Catal. B Environ.* **2019**, *245*, 522. doi: 10.1016/j.apcatb.2019.01.019.
(18) Wu, Y.; Wang, P.; Zhu, X.; Zhang, Q.; Wang, Z.; Liu, Y.; Zou, G.; Dai, Y.; Whangbo, M. H.; Huang, B., *Adv. Mater.* **2018**, *30*, 1704342. doi: 10.1002/adma.201704342.
(19) Liang, X.; Wang, P.; Li, M.; Zhang, Q.; Wang, Z.; Dai, Y.; Zhang, X.; Liu, Y.; Whangbo,

M. H.; Huang, B., *Appl. Catal. B Environ.* **2018**, *220*, 356. doi: 10.1016/j.apcatb.2017.07.075.
(20) Wu, Y.; Xing, M.; Tian, B.; Zhang, J.; Chen, F., *Chem. Eng. J.* **2010**, *16*, 710. doi: 10.1016/j.cej.2010.06.030.
(21) Dette, C.; Pérez-Osorio, M. A.; Kley, C. S.; Punke, P.; Patrick, C. E.; Jacobson, P.; Giustino, F.; Jung, S. J.; Kern, K., *Nano Lett.* **2014**, *14*, 6533. doi: 10.1021/nl503131s.
(22) Kumaravel, V.; Mathew, S.; Bartlett, J.; Pillai, S. C., *Appl. Catal. B Environ*. **2019**, *244*, 1021. doi: 10.1016/j.apcatb.2018.11.080.
(23) Dozzi, M. V.; Selli, E., *J. Photoch. Photobi. C* **2013**, *14*, 13. doi: 10.1016/j.jphotochemrev.2012.09.002.
(24) Yang, G.; Jiang, Z.; Shi, H.; Jones, M. O.; Xiao, T.; Edwards, P. P.; Yan, Z., *Appl. Catal. B Environ.* **2010**, *96*, 458. doi: 10.1016/j.apcatb.2010.03.004.
(25) Chen, X.; Burda, C., *J. Am. Chem. Soc.* **2008**, *130*, 5018. doi: 10.1021/ja711023z.
(26) Bangkedphol, S.; Keenan, H. E.; Davidson, C. M.; Sakultantimetha, A.; Sirisaksoontorn, W.; Songsasen, A., *J. Hazard. Mater.* **2010**, *184*, 533. doi: 10.1016/j.jhazmat.2010.08.068.
(27) In, S.; Orlov, A.; Berg, R.; García, F.; Pedrosa-Jimenez, S.; Tikhov, M. S.; Wright, D. S.; Lambert, R. M., *J. Am. Chem. Soc.* **2007**, *129*, 13790. doi: 10.1021/ja0749237.
(28) Zhang, Y. C.; Yang, M.; Zhang, G.; Dionysiou, D. D., *Appl. Catal. B Environ.* **2013**, *142*, 249. doi: 10.1016/j.apcatb.2013.05.023.
(29) Nursam, N. M.; Tan, J. Z. Y.; Wang, X.; Li, W.; Xia, F.; Caruso, R. A., *ChemistrySelect* **2016**, *1*, 4868. doi: 10.1002/slct.201601234.
(30) Li, D.; Haneda, H.; Hishita, S.; Ohashi, N., *Chem. Mater.* **2005**, *17*, 2588. doi: 10.1021/cm049100k.
(31) Di Li; Hajime Haneda; Shunichi Hishita, and; Ohashi, N., **2005**. *17*, 2596. doi: 10.1021/CM049099P.
(32) Yu, J. C.; Yu, J.; Ho, W.; Jiang, Z.; Zhang, L., *Chem. Mater.* **2002**, *14*, 3808. doi: 10.1021/cm020027c.
(33) Yu, J.; Xiang, Q.; Zhou, M., *Appl. Catal. B Environ.* **2009**, *90*, 595. doi: 10.1016/j.apcatb.2009.04.021.
(34) Sakthivel, S.; Shankar, M. V; Palanichamy, M.; Arabindoo, B.; Bahnemann, D. W.; Murugesan, V., *Water Res.* **2004**, *38*, 3001. doi: 10.1016/j.watres.2004.04.046.
(35) Yao, Z.; Jia, F.; Tian, S.; Li, C.; Jiang, Z.; Bai, X., *ACS Appl. Mater. Interfaces* **2010**, *2*, 2617. doi: 10.1021/am100450h.
(36) Pelaez, M.; Nolan, N. T.; Pillai, S. C.; Seery, M. K.; Falaras, P.; Kontos, A. G.; Dunlop, P. S. M.; Hamilton, J. W. J.; Byrne, J. A.; O'Shea, K.; et al., *Appl. Catal B Environ*. **2012**, *125*, 331. doi: 10.1016/j.apcatb.2012.05.036.
(37) Zhang, K.; Wang, X.; Guo, X.; He, T.; Feng, Y., *J. Nanoparticle Res.* **2014**, *16*, 2246. doi: 10.1007/s11051-014-2246-0.
(38) Kuvarega, A. T.; Krause, R. W. M.; Mamba, B. B., *J. Phys. Chem. C* **2011**, *115*, 22110. doi: 10.1021/jp203754j.
(39) He, Z.; Que, W.; Chen, J.; Yin, X.; He, Y.; Ren, J., *ACS Appl. Mater. Interfaces* **2012**, *4*, 6816. doi: 10.1021/am3019965.
(40) Sun, T.; Fan, J.; Liu, E.; Liu, L.; Wang, Y.; Dai, H.; Yang, Y.; Hou, W.; Hu, X.; Jiang, Z., *Powder Technol.* **2012**, *228*, 210. doi: 10.1016/j.powtec.2012.05.018.
(41) Linsebigler, A. L.; Lu, G.; Yates, J. T., *Chem. Rev.* **1995**, *95*, 735. doi: 10.1021/cr00035a013.

Draft

(42) Chang, W.; Yan, L.; Liu, B.; Sun, R., *Ceram. Int.* **2017**, *43*, 5881. doi: 10.1016/j.ceramint.2017.01.061.
(43) Li, W.; Jiang, N.; Hu, B.; Liu, X.; Song, F.; Han, G.; Jordan, T. J.; Hanson, T. B.; Liu, T. L.; Sun, Y., *Chem* **2018**, *4*, 637. doi: 10.1016/j.chempr.2017.12.019.
(44) Hamadanian, M.; Reisi-Vanani, A.; Behpour, M.; Esmaeily, A. S., *Desalination* **2011**, *281*, 319. doi: 10.1016/j.desal.2011.08.028.
(45) Xie, Y.; Li, Y.; Zhao, X., *J. Mol. Catal. A Chem.* **2007**, *277*, 119. doi: 10.1016/j.molcata.2007.07.031.
(46) Kaur, N.; Kaur, S.; Singh, V., *Desalin. Water Treat.* **2016**, *57*, 9237. doi: 10.1080/19443994.2015.1027956.
(47) Marczenko, Z. *Separation and Spectrophotometric Determination of Elements*; Ellis Horwood series in analytical chemistry; E. Horwood, 1986.
(48) Pelaez, M.; Nolan, N. T.; Pillai, S. C.; Seery, M. K.; Falaras, P.; Kontos, A. G.; Dunlop, P. S. M.; Hamilton, J. W. J.; Byrne, J. A.; O'Shea, K.; et al., *Appl. Catal. B Environ.* **2012**, *125*, 331. doi: 10.1016/j.apcatb.2012.05.036.
(49) Mahesh, K. P. O.; Kuo, D.-H.; Huang, B.-R.; Ujihara, M.; Imae, T., *Appl. Catal. A Gen.* **2014**, *475*, 235. doi: 10.1016/j.apcata.2014.01.044.
(50) O'Regan, B.; Grätzel, M., *Nature* **1991**, *353*, 737. doi: 10.1038/353737a0.
(51) Alothman, Z. A., *Materials*. **2012**, *5*, 2874. doi: 10.3390/ma5122874.
(52) Herrmann, J.-M., *Catal. Today* **1999**, *53*, 115. doi: 10.1016/S0920-5861(99)00107-8.
(53) Parmon, V.; Emeline, A. V; Serpone, N., *J. Photochem. Photobiol. A Chem.* **2002**, *4*, 91. doi: 10.1016/S1010-6030(01)00659-1.
(54) Konstantinou, I. K.; Albanis, T. A., *Appl. Catal. B Environ.* **2004**, *49*, 1. doi: 10.1016/J.APCATB.2003.11.010.
(55) Ishibashi, K.; Fujishima, A.; Watanabe, T.; Hashimoto, K., *J. Photochem. Photobiol. A Chem.* **2000**, *134*, 139. doi: 10.1016/S1010-6030(00)00264-1.
(56) Gözmen, B.; Turabik, M.; Hesenov, A., *J. Hazard. Mater.* **2009**, *164*, 1487. doi: 10.1016/J.JHAZMAT.2008.09.075.
(57) Neren Ökte, A.; Yilmaz, Ö., *Appl. Catal. B Environ.* **2008**, *85*, 92. doi: 10.1016/j.apcatb.2008.07.025.
(58) Xu, S.; Zhu, Y.; Jiang, L.; Dan, Y., *Water. Air. Soil Pollut.* **2010**, *213*, 151. doi: 10.1007/s11270-010-0374-4.
(59) Hoffmann, M. R.; Martin, S. T.; Choi, W.; Bahnemann, D. W., *Chem. Rev.* **1995**, *95*, 69. doi: 10.1021/cr00033a004.
(60) Kosmulski, M., *Adv. Colloid Interface Sci.* **2002**, *99*, 255. doi: 10.1016/S0001-8686(02)00080-5.
(61) Fu, H.; Lu, G.; Li, S., *J. Photochem. Photobiol. A Chem.* **1998**, *114*, 81. doi: 10.1016/S1010-6030(98)00205-6.
(62) Giménez, J.; Aguado, M. A.; Cervera-March, S., *J. Mol. Catal. A Chem.* **1996**, *105*, 67. doi: 10.1016/1381-1169(95)00148-4.
(63) Konstantinou, I. K.; Albanis, T. A., *Appl. Catal. B Environ.* **2004**, *49*, 1. doi: 10.1016/j.apcatb.2003.11.010.
(64) Akpan, U. G.; Hameed, B. H., *J. Hazard. Mater.* **2009**, *170*, 520. doi: 10.1016/j.jhazmat.2009.05.039.

Draft

Figures caption list:

Fig. 1 XRD pattern of undoped TiO_2 (a) and FFeTS (b)
Fig. 2 FT-IR spectra of undoped TiO_2 (a) and FFeTS (b)
Fig. 3 DRS spectra of undoped TiO_2 (a) and FFeTS (b)
Fig. 4 FESEM images of undoped TiO_2 (a) and FFeTS (b)
Fig. 5 EDX pattern of FFeTS nanocomposites
Fig. 6 TEM images of FFeTS nanocomposites
Fig. 7 N_2 adsorption/desorption isotherm of FFeTS nanocomposites. Inset: BJH pore size distribution curve of FFeTS
Fig. 8 Schematic illustration denoting simultaneous photocatalytic removal of the pollutants by TiO_2
Fig. 9 Effect of pH on removal percentage of the pollutants in presence of FFeTS
Fig. 10 Effect of flow rate on removal percentage of the pollutants in presence of FFeTS
Fig. 11 Effect of photoreactor vessels' angle against solar light on removal percentage of the pollutants in presence of FFeTS
Fig. 12 Removal percentages of the pollutants under visible light in presence of FFeTS, in presence of pristine TiO_2/SiO_2, at dark condition and in the absence of FFeTS; *ABS: Absence of photocatalyst, TS: Pristine TiO_2/SiO_2*
Fig. 13 Removal percentages of the pollutants under solar light in presence of FFeTS, in presence of pristine TiO_2/SiO_2 and in the absence of FFeTS; *ABS: Absence of photocatalyst, TS: Pristine TiO_2/SiO_2*
Fig. 14 Removal percentages of the pollutants under visible light in presence of F-TiO_2/SiO_2 and Fe-TiO_2/SiO_2
Fig. 15 Removal percentages of the pollutants under solar light in presence of F-TiO_2/SiO_2 and Fe-TiO_2/SiO_2
Fig. 16 Removal percentages of the pollutants under solar irradiation at semi-cloudy condition
Fig. 17 Repeatability (a) and durability (b) experiments of the prepared substrates

Draft

Table legend list:

Table 1
Physical properties of the prepared samples

Draft

Table 1

Samples	BET surface area (S_{BET}) (m^2 g^{-1})	Average pore diameter (nm)
TiO_2	39.60	5.77
F-Fe-TiO_2	77.48	10.60
FFeTS	325.67	6.60

Draft

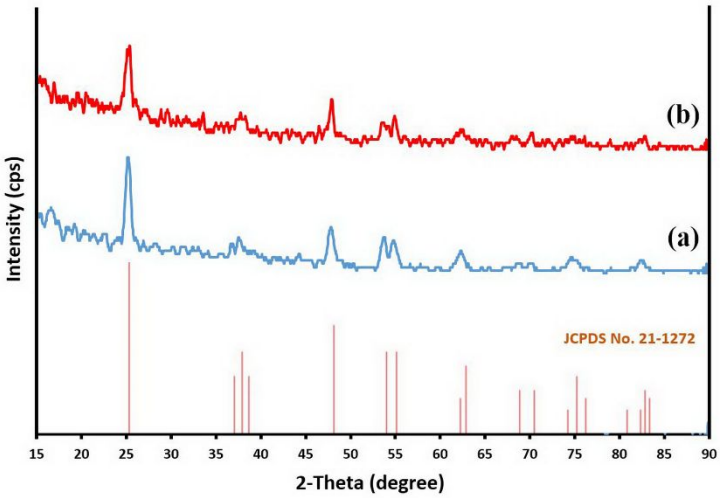
(b)
(a)
JCPDS No. 21-1272
Intensity (cps)
15 20 25 30 35 40 45 50 55 60 65 70 75 80 85 90
2-Theta (degree)

Fig. 1

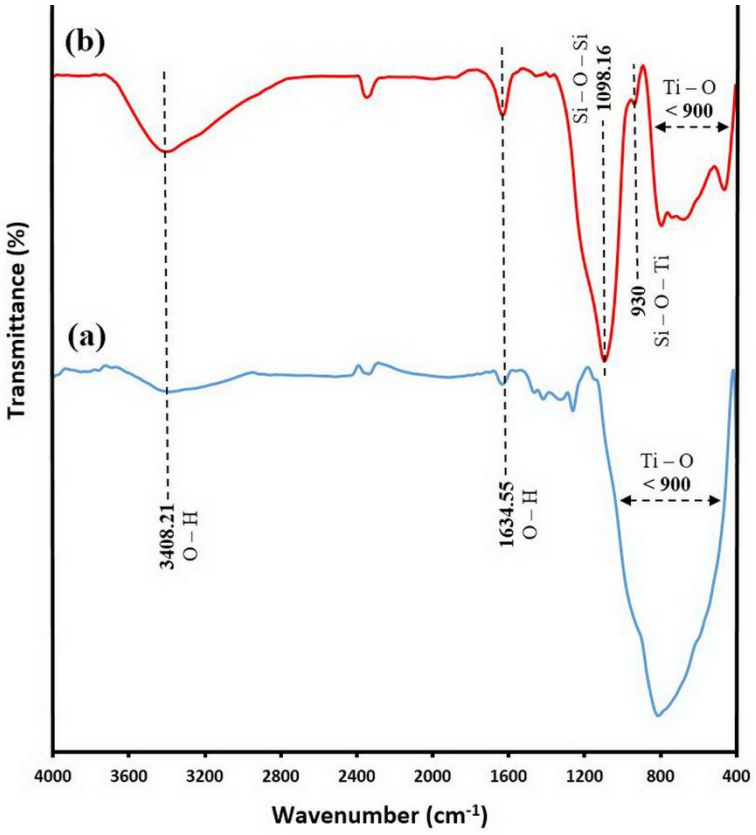
(b)
(a)
Transmittance (%)
3408.21
O – H
1634.55
O – H
Si – O – Si
1098.16
930
Si – O – Ti
Ti – O
< 900
Ti – O
< 900
4000
3600
3200
2800
2400
2000
1600
1200
800
400
Wavenumber (cm-1)

Fig. 2

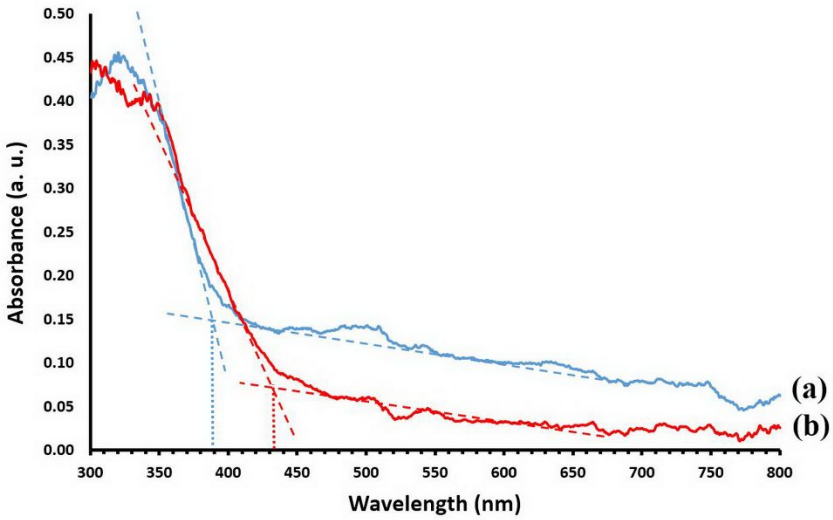
0.50
0.45
0.40
0.35
0.30
0.25
0.20
0.15
0.10
0.05
0.00
Absorbance (a. u.)
300
350
400
450
500
550
600
650
700
750
800
Wavelength (nm)
(a)
(b)

Fig. 3

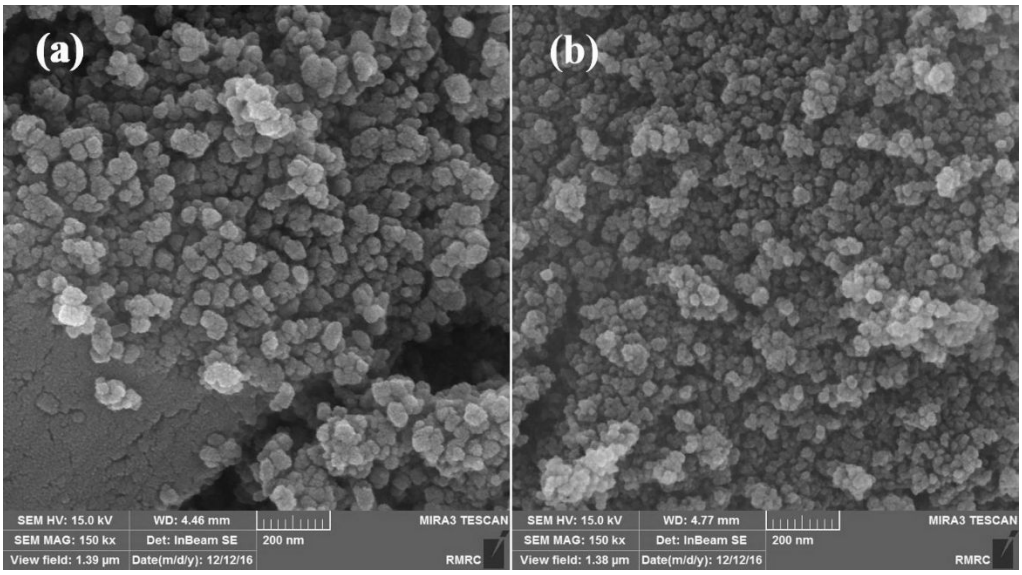
(a)
SEM HV: 15.0 kV
WD: 4.46 mm
MIRA3 TESCAN
SEM MAG: 150 kx
Det: InBeam SE
200 nm
View field: 1.39 µm
Date(m/d/y): 12/12/16
RMRC
(b)
SEM HV: 15.0 kV
WD: 4.77 mm
MIRA3 TESCAN
SEM MAG: 150 kx
Det: InBeam SE
200 nm
View field: 1.38 µm
Date(m/d/y): 12/12/16
RMRC

Fig. 4

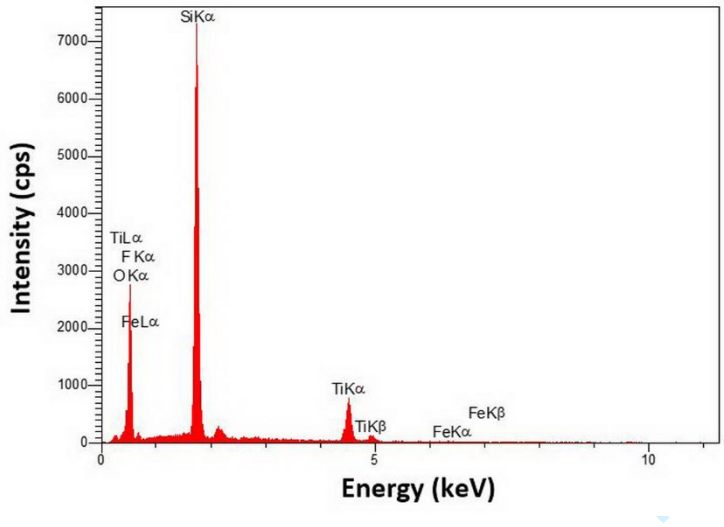
SiKα
TiLα
F Kα
O Kα
FeLα
TiKα
TiKβ
FeKα
FeKβ
Intensity (cps)
Energy (keV)
0
1000
2000
3000
4000
5000
6000
7000
0
5
10

Fig. 5

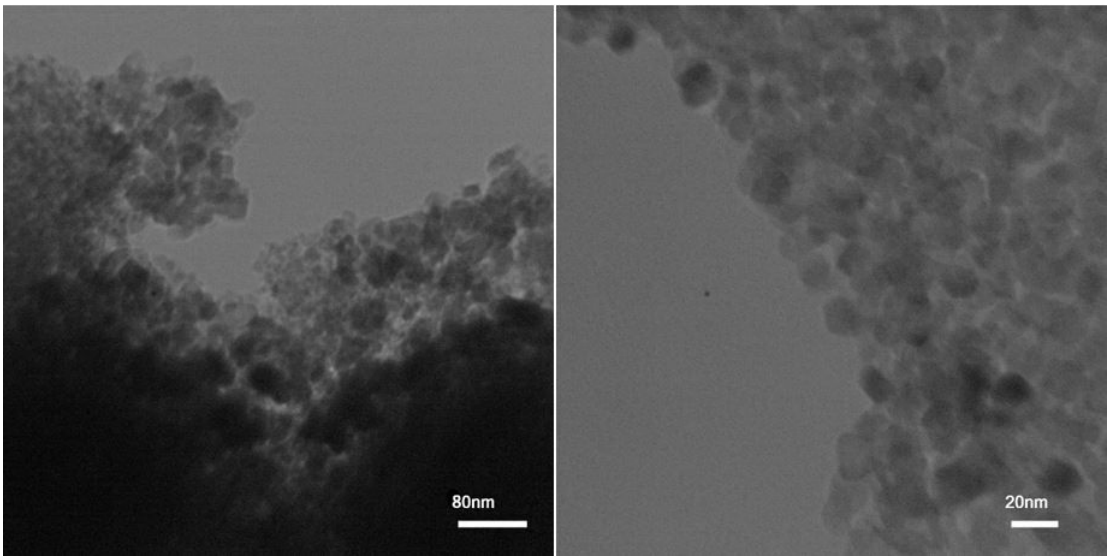

Fig. 6

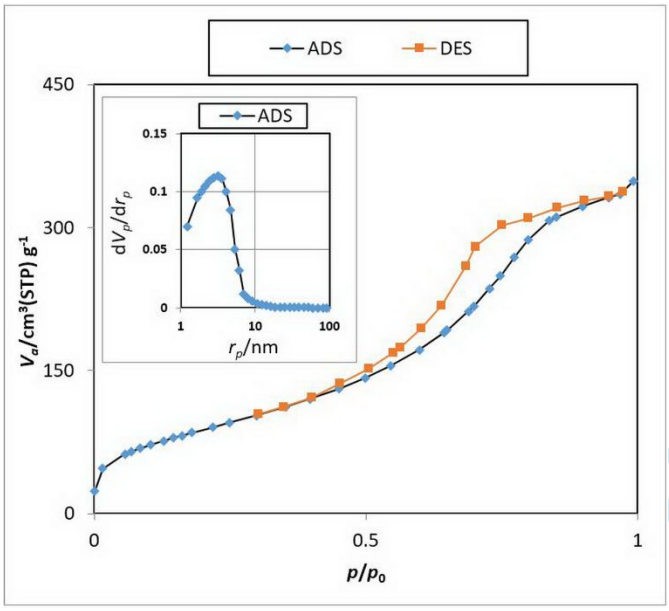
ADS
DES
450
300
150
0
0
0.5
1
V_a/cm³(STP) g⁻¹
p/p₀
ADS
0.15
0.1
0.05
0
1
10
100
dV_p/dr_p
r_p/nm

Fig. 7

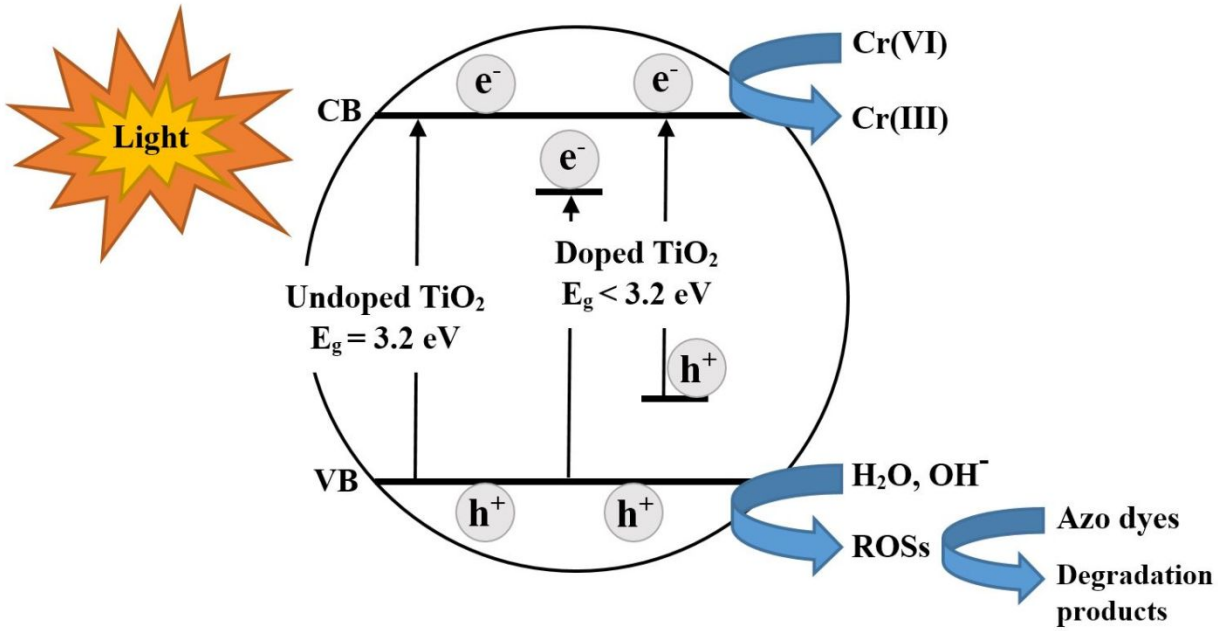
Light
CB
VB
e-
e-
e-
h+
h+
h+
Undoped TiO2
Eg = 3.2 eV
Doped TiO2
Eg < 3.2 eV
Cr(VI)
Cr(III)
H2O, OH-
ROSs
Azo dyes
Degradation products

Fig. 8

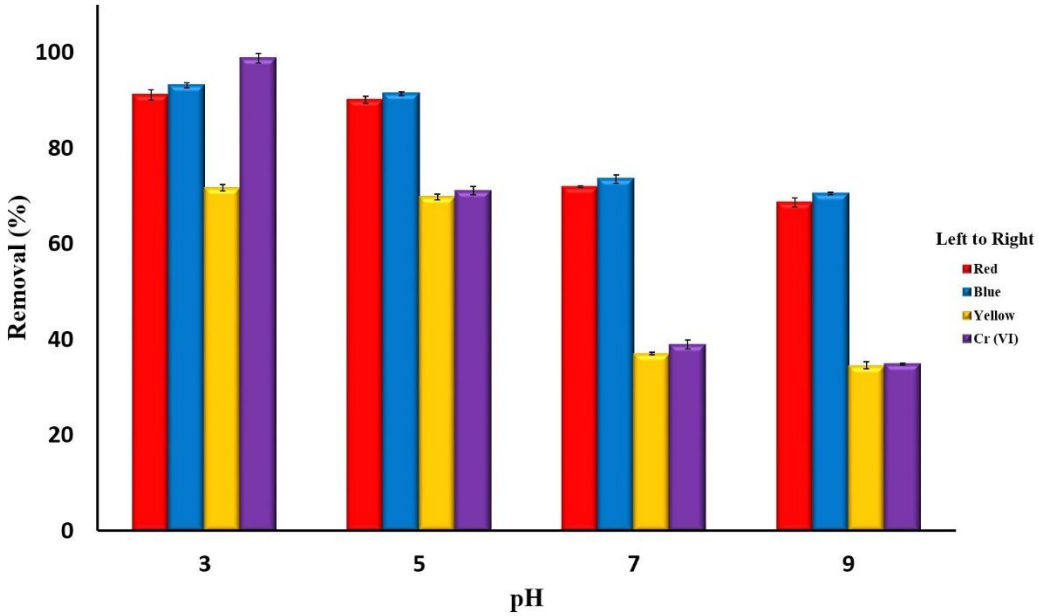
100
80
60
40
20
0
Removal (%)
3
5
7
9
pH
Left to Right
Red
Blue
Yellow
Cr (VI)

Fig. 9

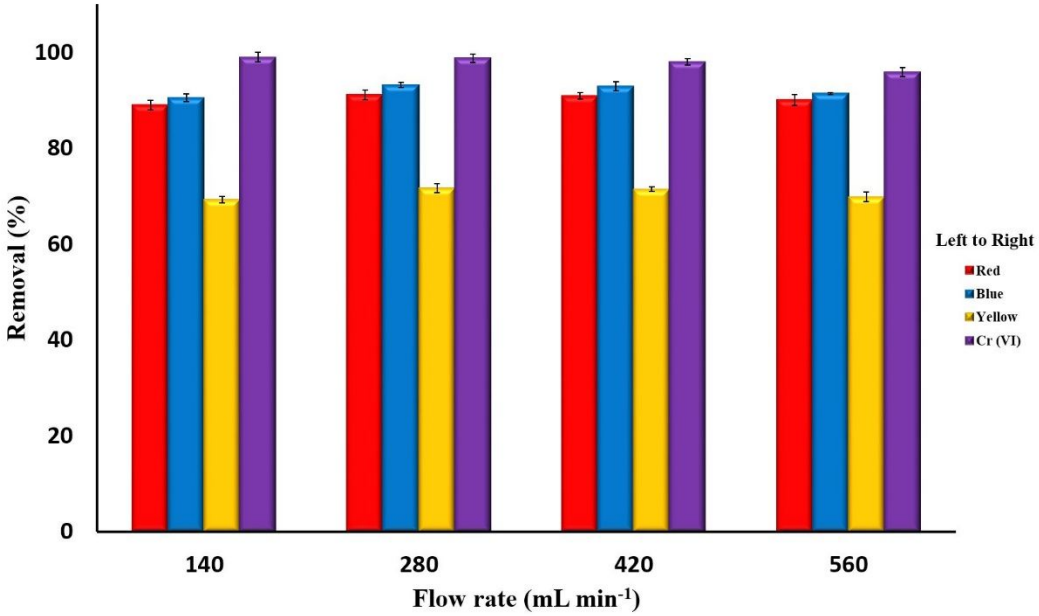
100
80
60
40
20
0
Removal (%)
140
280
420
560
Flow rate (mL min-1)
Left to Right
Red
Blue
Yellow
Cr (VI)

Fig. 10

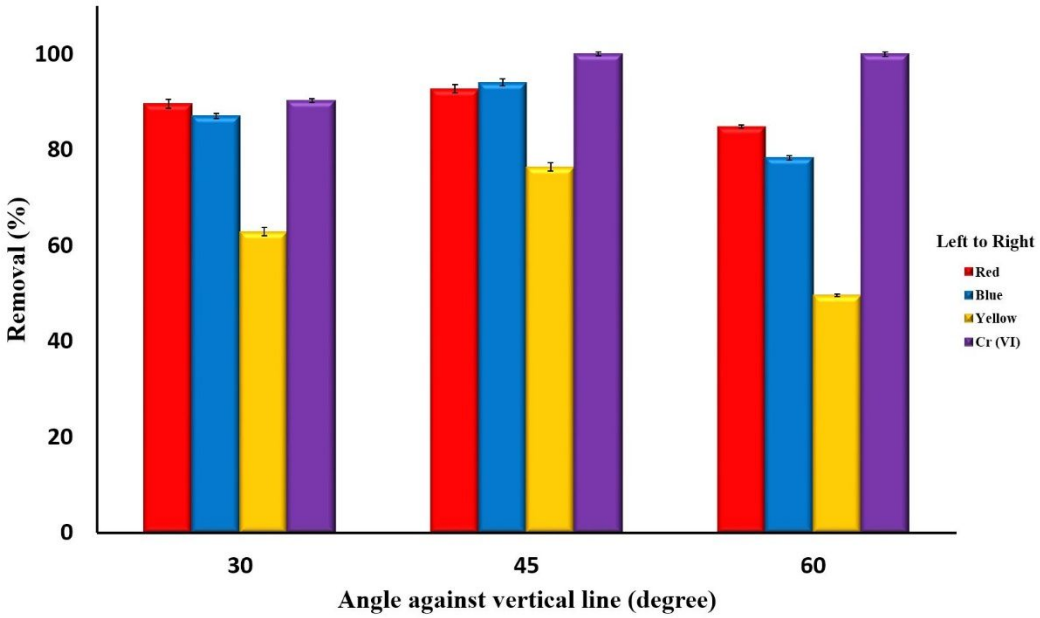
100
80
60
40
20
0
Removal (%)
30
45
60
Angle against vertical line (degree)
Left to Right
Red
Blue
Yellow
Cr (VI)

Fig. 11

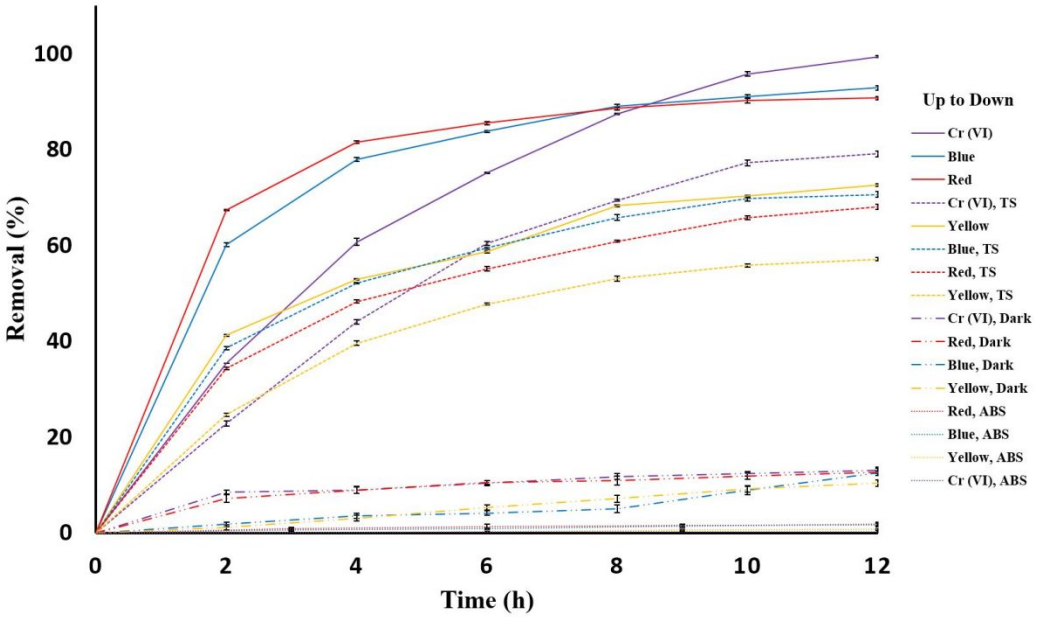
Removal (%)
Time (h)
0
20
40
60
80
100
0
2
4
6
8
10
12
Up to Down
Cr (VI)
Blue
Red
Cr (VI), TS
Yellow
Blue, TS
Red, TS
Yellow, TS
Cr (VI), Dark
Red, Dark
Blue, Dark
Yellow, Dark
Red, ABS
Blue, ABS
Yellow, ABS
Cr (VI), ABS

Fig. 12

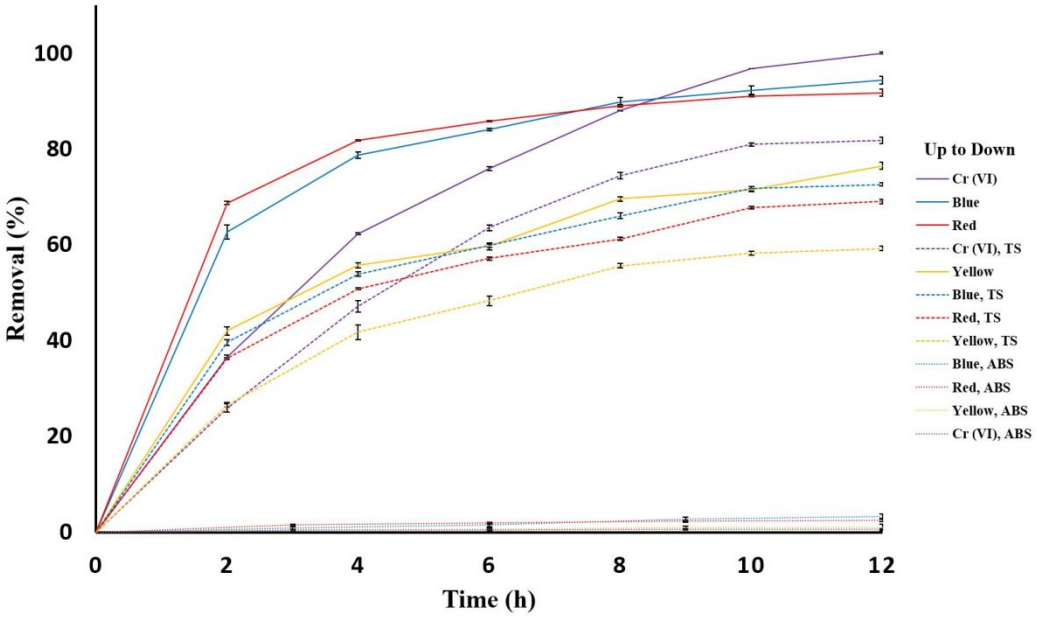
Removal (%)
Time (h)
0
20
40
60
80
100
0
2
4
6
8
10
12
Up to Down
Cr (VI)
Blue
Red
Cr (VI), TS
Yellow
Blue, TS
Red, TS
Yellow, TS
Blue, ABS
Red, ABS
Yellow, ABS
Cr (VI), ABS

Fig. 13

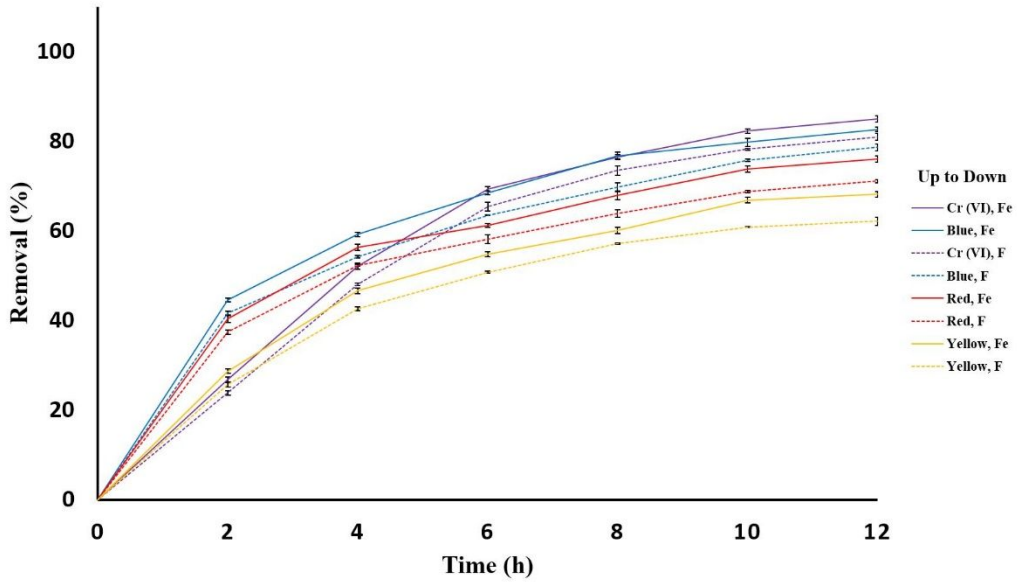
100
80
60
40
20
0
Removal (%)
0
2
4
6
8
10
12
Time (h)
Up to Down
Cr (VI), Fe
Blue, Fe
Cr (VI), F
Blue, F
Red, Fe
Red, F
Yellow, Fe
Yellow, F

Fig. 14

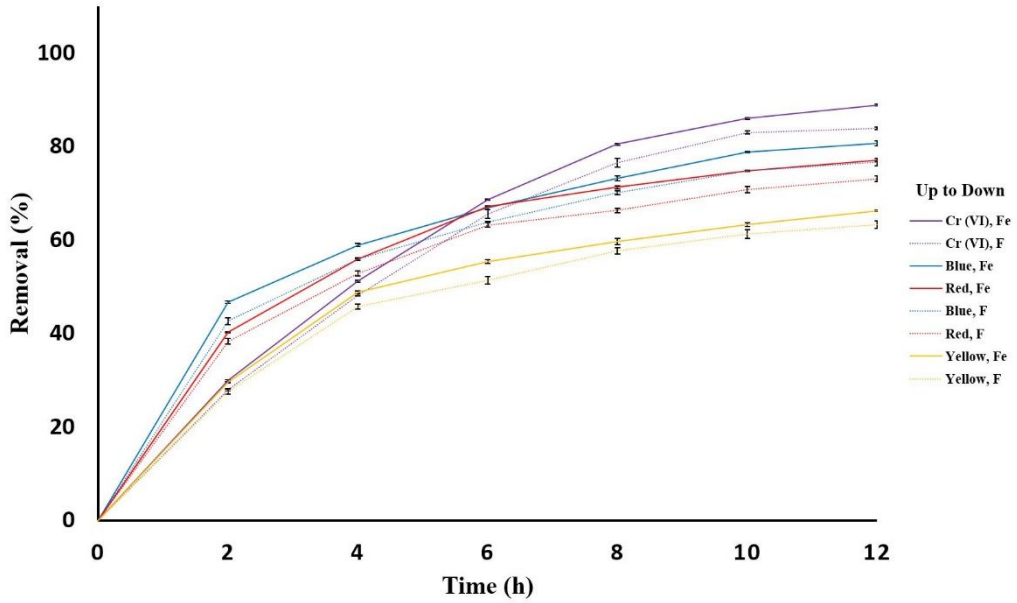
Removal (%)
100
80
60
40
20
0
0
2
4
6
8
10
12
Time (h)
Up to Down
Cr (VI), Fe
Cr (VI), F
Blue, Fe
Red, Fe
Blue, F
Red, F
Yellow, Fe
Yellow, F

Fig. 15

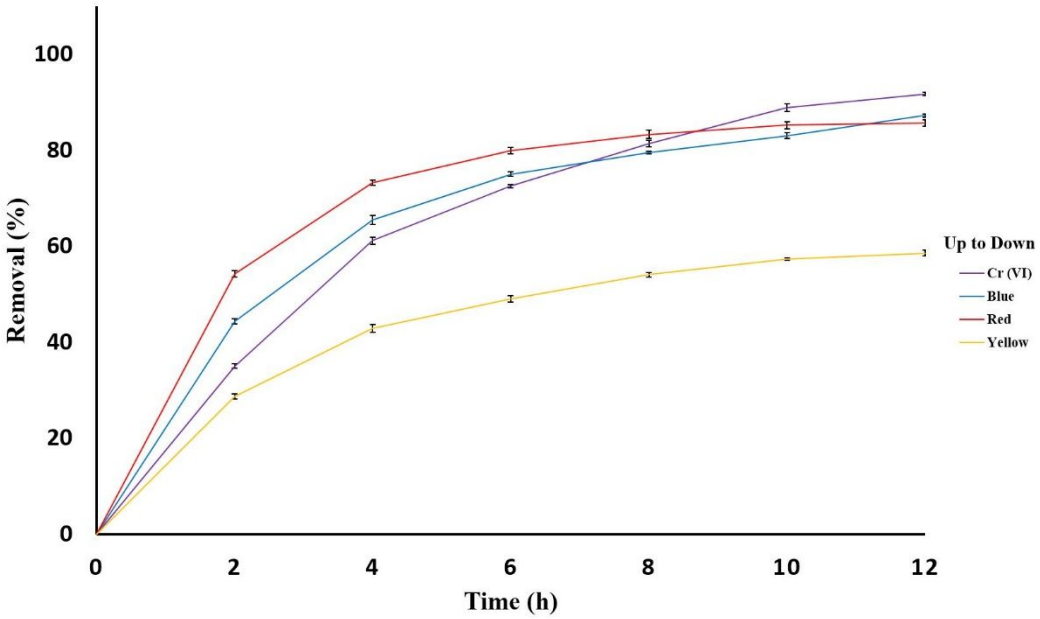
100
80
60
40
20
0
Removal (%)
0
2
4
6
8
10
12
Time (h)
Up to Down
Cr (VI)
Blue
Red
Yellow

Fig. 16

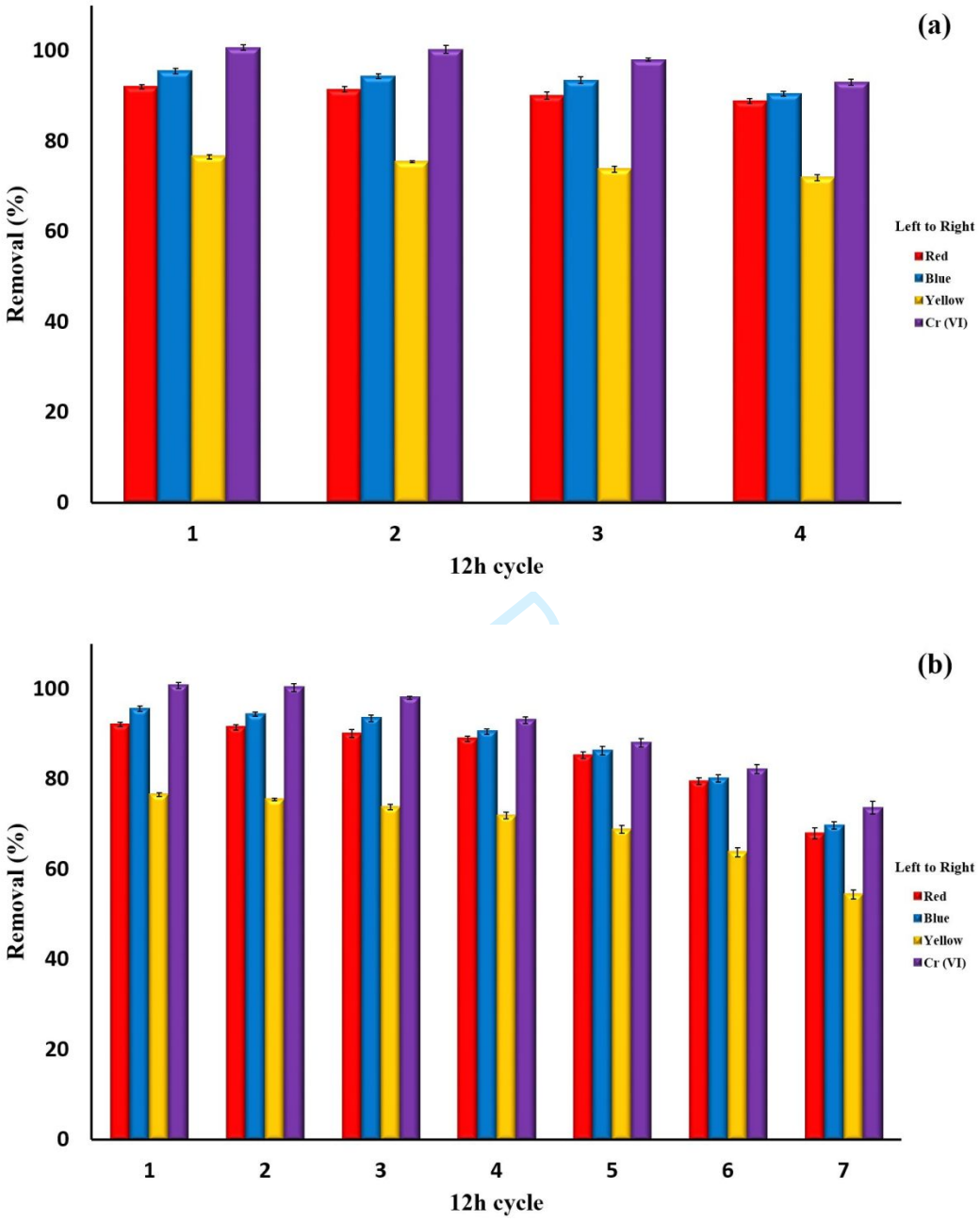
(a)
Removal (%)
100
80
60
40
20
0
1
2
3
4
12h cycle
Left to Right
Red
Blue
Yellow
Cr (VI)
(b)
Removal (%)
100
80
60
40
20
0
1
2
3
4
5
6
7
12h cycle
Left to Right
Red
Blue
Yellow
Cr (VI)

Fig. 17